The American Journal of Pathology, Vol. 171, No. 5, November 2007

DOI: 10.2353/ajpath.2007.060968

Tumorigenesis and Neoplastic Progression

Caveolin-1 Is Critical for the Maturation of Tumor Blood Vessels through the Regulation of Both Endothelial Tube Formation and Mural Cell Recruitment

Julie DeWever,* Françoise Frérart,* Caroline Bouzin,* Christine Baudelet,† Réginald Ansiaux,† Pierre Sonveaux,* Bernard Gallez,† Chantal Dessy,* and Olivier Feron*

From the Unit of Pharmacology and Therapeutics (UCL-FATH 5349), and the Biomedical Magnetic Resonance Unit,† Université catholique de Louvain, Brussels, Belgium*

In the normal microvasculature, caveolin-1, the structural protein of caveolae, modulates transcytosis and paracellular permeability. Here, we used caveolin-1-deficient mice ($Cav^{-/-}$) to track the potential active roles of caveolin-1 down-modulation in the regulation of vascular permeability and morphogenesis in tumors. In B16 melanoma-bearing $Cav^{-/-}$ mice, we found that fibrinogen accumulated in early-stage tumors to a larger extent than in wild-type animals. These results were confirmed by the observations of a net elevation of the interstitial fluid pressure and a relative deficit in albumin extravasation in $Cav^{-/-}$ tumors (versus healthy tissues). Immunostaining analyses of $Cav^{-/-}$ tumor sections further revealed a higher density of CD31-positive vascular structures and a dramatic deficit in α-smooth muscle actin-stained mural cells. The increase in blood plasma volume in $Cav^{-/-}$ tumors was confirmed by dynamic contrast enhanced-magnetic resonance imaging and found to be associated with a more rapid tumor growth. Finally, an *in vitro* wound test and the aorta ring assay revealed that silencing caveolin expression could directly impair the migration and the outgrowth of smooth muscle cells/pericytes, particularly in response to platelet-derived growth factor. In conclusion, a decrease in caveolin abundance, by promoting angiogenesis and preventing its termination by mural cell recruitment, appears as an important control point for the formation of new tumor blood vessels. Caveolin-1 therefore has the potential to be a marker of tumor vasculature maturity that may help adjusting anticancer therapies. ***(Am J Pathol 2007, 171:1619–1628; DOI: 10.2353/ajpath.2007.060968)***

The tumor vasculature is structurally abnormal, with poor fitting into the usual classification of arterioles, capillaries, or venules.[1] Many tumor vessels have an irregular diameter and present an abnormal branching pattern.[2] The endothelium lining these vessels present intercellular gaps, transendothelial holes, and vesiculo-vacuolar organelles.[3,4] These structural alterations account for one key feature of tumor biology, namely the vascular leakiness[1] that itself correlates with the histological grade and the metastatic potential of tumors.[4,5] The above morphological view of the tumor vessel permeability, and the associated increase in interstitial fluid pressure (IFP),[6] may, however, lead to overlooking that these alterations are governed by biochemical mechanisms. Different pharmacological treatments interfering with major signaling pathways have proved their efficacy in reducing elevated tumor IFP and vessel leakiness. For instance, a vascular endothelial growth factor (VEGF) monoclonal antibody was shown to dramatically reduce tumor IFP both in mice and in patients, leading to the concept of tumor vessel normalization.[7] Reduction in extracellular matrix formation by transforming growth factor-β antagonists[8] or resistance in vessel leakiness by angiopoietin overexpression[9] are other examples of the dynamics of the tumor vascular permeability.

The reversibility of the biological pathways supporting the tumor vessel leakiness led us to examine the role of

Supported by the Fonds Spécial de la Recherche, the Fonds de la Recherche Scientifique Médicale, the Fonds National de la Recherche Scientifique, the Télévie, the Belgian Federation Against Cancer, the J. Maisin Foundation, and an Action de Recherche Concertée from the Communauté Française de Belgique (no. 04/09-317).

Accepted for publication August 3, 2007.

O.F. and C.D. are Fonds National de la Recherche Scientifique Senior Research Associates.

Address reprint requests to Olivier Feron, University of Louvain Medical School, Unit of Pharmacology and Therapeutics (UCL-FATH 5349), 52 Ave E. Mounier, B-1200 Brussels, Belgium. E-mail: olivier.feron@uclouvain.be.

caveolin in this process. Caveolin is the structural protein of vesicle-like plasmalemmal microdomains termed caveolae that are involved in transcytosis, ie, the transcellular movement of macromolecules from the luminal side of capillary endothelial cells to the interstitial space.[10] Through the regulation of intercellular interactions, caveolin is also a modulator of endothelial barrier integrity.[11] Whether this capacity to regulate physiological vascular permeability is also involved in tumor vessel leakiness is primarily unexplored.

In the cardiovascular context, we and others have previously documented that the recombinant expression of caveolin[12] or the administration of caveolin-derived peptides[13] exert anti-angiogenic effects through the inhibition of the endothelial nitric-oxide synthase (eNOS). Caveolin has also been shown to co-purify with the VEGF-R2 receptor in caveolae and thereby to modulate VEGF signaling.[14,15] Interestingly, endogenous (native) caveolin has been reported to be down-regulated in the tumor vasculature[16] and in endothelial cells exposed to angiogenic growth factors including VEGF and basic fibroblast growth factor[17,18] or when co-cultured with tumor cells.[16] Angiogenic mediators such as nitric oxide[19] or proangiogenic stresses such as ionizing radiation[20] and hypoxia[16] have also been associated with a decrease in endothelial caveolin abundance. Conversely, angiogenesis inhibitors including angiostatin, fumagillin, and thalidomide were reported to block VEGF-induced down-regulation of caveolin-1.[17]

In this study, we used caveolin-deficient mice bearing B16 melanoma to evaluate the hypothesis of an active role of the caveolin down-regulation in the modulation of tumor vessel permeability and angiogenesis. By means of a variety of *in vitro* and *in vivo* techniques including immunohistochemistry and dynamic contrast enhanced-magnetic resonance imaging (DCE-MRI) to evaluate the structural/functional characteristics of the tumor vasculature, we found that angiogenesis was orchestrated in tumors grown in $Cav^{-/-}$ mice via the extravasation of plasma proteins leading to the constitution of a provisional matrix required for endothelial tube formation and the deficit in smooth muscle cell (SMC)/pericyte recruitment, thereby preventing the tumor vessel maturation and the termination of the neovascularization process.

Materials and Methods

Mouse Model and Cells

Cav-1-deficient ($Cav^{-/-}$) mice (originally obtained from Drs. M. Drab and T.V. Kurzchalia, Max Planck Institute for Molecular Cell Biology and Genetics, Dresden, Germany) and their control littermates ($Cav^{+/+}$) were generated through heterozygous mating and housed in our local facility. A minimum of six backcrossings was performed before using the animals described in this study. We used 8- to 10-week-old animals that were subcutaneously injected into the left flank with 10^6 B16 melanoma cells; tumor diameters were determined with an electronic caliper. In some experiments, luciferase-encoding B16 melanoma cells (Xenogen, Hopkinton, MA) were used to track early appearance of tumor mass; a single dose of luciferin (150 mg/kg) was injected intraperitoneally into anesthetized mice and *in vivo* bioluminescence was detected 15 minutes later on an IVIS50 imaging system (Xenogen). These procedures were approved by the local authorities according to national animal care regulations.

Melanoma (B16-F10) cells and 10T1/2 cells (SMC/pericyte progenitors) were routinely cultured in serum containing Dulbecco's modified Eagle's medium and Eagle's basal medium, respectively. 10T1/2 cells were always maintained at a confluence level <80 to 90% and used between passages 5 and 15. Both cell types were from the American Type Culture Collection (Manassas, VA). In some experiments, SMCs/myofibroblasts were also derived from aorta strips, as previously reported[21]; more than 90% of the cells isolated through this procedure were found to be positive for α-SMA staining, and less than 1% were CD31-positive.

Immunostaining

Collected tumors were cryosliced and probed with antibodies against fibrinogen/fibrinogen degradation products or α-SMA (both from DAKO, Heverlee, Belgium) and against CD31 (BD Pharmingen, Lexington, KY). 10T1/2 cells were stained with caveolin antibodies (BD Pharmingen) and fluorescein isothiocyanate (FITC)-labeled phalloidin (Sigma). 4,6-Diamidino-2-phenylindole (DAPI)-containing mounting medium (Vector Laboratories Inc., Burlingame, CA) was used to stain the nuclei. Secondary antibodies were coupled to tetramethyl-rhodamine isothiocyanate (TRITC) or FITC fluorophores (Jackson, De Pinte, Belgium). Tumor slices or cells were examined with an Axioskop microscope (Zeiss, Wetzlar, Germany) equipped for fluorescence.

In Vivo *Albumin Clearance*

^{125}I-Albumin was prepared by classical radioiodination. Briefly, serum albumin (20%; Croix Rouge, Brussels, Belgium) was incubated in the presence of carrier-free ^{125}I (2 mCi; MDS Nordion, Fleurus, Belgium), using chloramine as oxidizing agent and $Na_2S_2O_5$ to stop the reaction. The labeled protein was purified by permeation gel chromatography (Sephadex G-25, NAP 25 column; Amersham Biosciences, Uppsala, Sweden) and then sterilized by filtration on a ministart filter (0.2 μm; Sartorius, Goettingen, Germany). The radiochemical purity monitored by paper chromatography was higher than 99%. For animal experiments, 10^6 dpm of the ^{125}I-albumin solution was injected in the tail vein. Sixty minutes after injection, mice were sacrificed, and tumors were microdissected and weighted. The amount of ^{125}I-albumin in each tissue sample was then determined using a 1480 Wizard counter (Wallac, Turku, Finland).

IFP Measurements

IFP was measured using a wick-in-needle apparatus, as previously described.[22] Measurements were done by in-

serting the needle into the center of the tumor and injecting 50 μl of 0.9% sodium chloride to ensure fluid communication between the tumor and the pressure monitor system. Large-size tumors are needed for these measurements, and in this study, only 9-mm-diameter tumors were used to evaluate IFP.

DCE-MRI

This technique was used to compare tumor perfusion and vascular permeability in tumor-bearing mice, as previously described.[23–26] In brief, MRI was obtained with a 4.7-T (200 MHz, ^{1}H) 40-cm inner diameter bore system (Bruker Biospec, Ettlingen, Germany) using the 6.5-kDa blood pool contrast agent P792 (Vistarem, Guerbet, France). High-resolution multislice T2-weighted spin echo anatomical imaging was performed just before dynamic contrast-enhanced imaging. The tracer concentration changes were fitted to a two-compartment pharmacokinetics model as previously described.[23,27,28] An operator-defined region of interest encompassing the tumor was analyzed on a voxel-by-voxel basis to obtain parametric maps. The K_{trans} and K_{ep} values (min^{-1}) reflect the influx volume transfer constant from the plasma to the interstitial space and the fractional rate of efflux from the interstitial space back to the blood, respectively. V_p is the blood plasma volume per unit volume of tissue. The fraction of perfused tumor was defined as the number of voxels with statistical significance for K_{trans} divided by the total number of voxels in the whole tumor region of interest.

siRNA Transfection and Immunoblotting

10T1/2 cells were transfected with duplex short interferring (si)RNA targeting caveolin-1 (corresponding to coding sequences 206 to 226 and 286 to 306) using Lipofectin (Invitrogen, Carlsbad, CA), according to the manufacturer's protocol. A scramble siRNA was used as control and specific reduction of caveolin-1 expression level was confirmed by immunoblotting of 10T1/2 cell lysates with caveolin antibodies (BD Pharmingen). Anti-Akt and anti-phospho-Akt (Ser473) antibodies (Cell Signaling, Beverly, MA) were also used to immunoblot SMC/myofibroblast lysates.

To evaluate possible changes in caveolin expression within the vasculature of growing tumors, we also used lysates of microdissected tumor blood vessels, as previously described.[29,30] In brief, B16 melanoma cells were injected at the vicinity of the saphenous arteriole in one of the rear legs. The arteriole and the downstream branches (diameters between 100 and 200 μm) were progressively trapped in the growing tumor mass. After 2 weeks, tumor-co-opted vessels and size-matched healthy arterioles from the contralateral leg were microdissected, lysed, and immunoblotted with caveolin-1 antibodies. The microvessels from five mice were pooled to get enough material for immunodetection.

In Vitro *Migration and* ex Vivo *Angiogenesis Assay*

To evaluate 10T1/2 cell migration, a 0.5-mm-wide line was scraped across confluent serum-starved cells. For the quantitative analysis, a migration index was defined as the ratio (expressed as percentage) of the density of migrating cells (observed 24 hours after the wound) in the center of the wounded area versus the density of cells in size-matched area of the unwounded region.[20] To evaluate *ex vivo* angiogenesis, aortic rings (obtained from $Cav^{-/-}$ and $Cav^{+/+}$ mice) were embedded in rat tail collagen gel and cultured for 12 days in MCDB131 medium supplemented with 5% autologous serum, as previously described.[31] Cell migration and endothelial tube formation were observed through an inverted phase contrast microscope and quantified by two blinded investigators using images randomly captured by a video camera system.

Statistical Analyses

Statistical analyses were made using Student's *t*-tests except for the fibrinogen accumulation scoring (Wilcoxon two-sample test) and for the tumor growth (two-way analysis of variance test).

Results

$Cav^{-/-}$ Mice Present an Elevated Vascular Permeability to Albumin in Healthy Tissue but Not in Established Tumors

We first used radioiodinated albumin (^{125}I-albumin) to have an instant picture of the acute permeability status of B16 melanoma established in caveolin-1-deficient ($Cav^{-/-}$) mice or in the wild-type littermates ($Cav^{+/+}$). One hour after ^{125}I-albumin intravenous administration to B16 melanoma-bearing mice, blood, skeletal muscle,

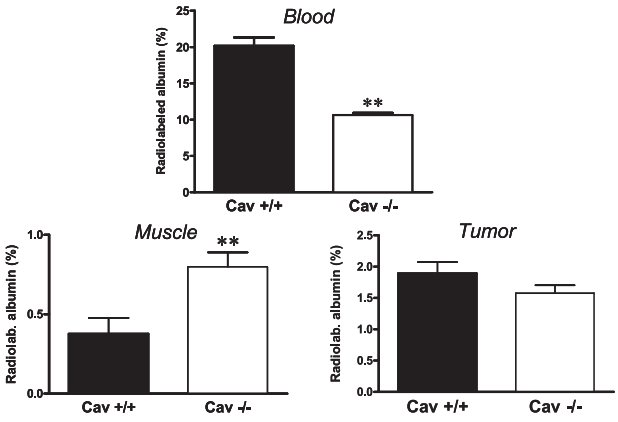

Figure 1. Permeability to albumin is increased in $Cav^{-/-}$ healthy tissues but not in tumors. ^{125}I-Albumin was injected in the tail vein of B16 melanoma-bearing $Cav^{+/+}$ or $Cav^{-/-}$ mice; the animals were sacrificed 1 hour later. Bar graphs represent the extent of ^{125}I-albumin cleared from blood and accumulated in skeletal muscle and in tumors; data (normalized for the tissue weight) are expressed as the percent of the total amount of injected radioactivity ($^{**}P < 0.01$, $n = 5$).

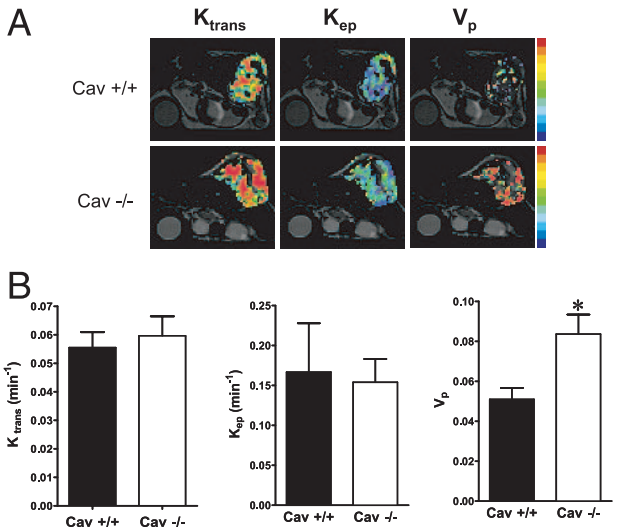

Figure 2. Parametric mapping by DCE-MRI reveals an increased blood plasma volume in Cav$^{-/-}$ tumors. **A:** Typical parametric MR images of K_{trans} (influx constant from the plasma to the interstitium), K_{ep} (fractional rate of efflux from the interstitium), and V_p (blood plasma volume per unit volume of tumor) from 6-mm-diameter B16 melanoma established in Cav$^{+/+}$ or Cav$^{-/-}$ mice. **B:** Quantitative analyses of the indicated pharmacokinetic parameters; data are expressed as means ± SEM (*$P < 0.05$, $n = 5$ to 6).

and tumor samples were collected. As shown in Figure 1, blood clearance of ^{125}I-albumin appeared significantly greater ($P < 0.01$) in Cav$^{-/-}$ mice. This indication of a global increase in vascular permeability in Cav$^{-/-}$ mice was further confirmed by the higher accumulation of radioactivity in peripheral tissues such as skeletal muscle ($P < 0.01$) (versus Cav$^{+/+}$ mice). By contrast, accumulation in size-matched (6-mm diameter) tumors reached similar levels in both mouse genotypes (Figure 1).

DCE-MRI Reveals an Increased Blood Plasma Volume in Large Tumors Established in Cav$^{-/-}$ Mice but No Apparent Difference in Vessel Leakiness

Tumor vessel permeability and perfusion were also monitored in both mouse genotypes via dynamic contrast-enhanced MRI using intravenous infusion of the macromolecular blood-pool agent P792 (Figure 2A). Both influx and efflux parameters, K_{trans} and K_{ep}, did not significantly differ between tumor-bearing Cav$^{-/-}$ and Cav$^{+/+}$ mice, indicating that the overall tumor vessel permeability was similar in the two mouse genotypes (Figure 2B). By contrast, the plasmatic volume fraction (V_p) was significantly higher in Cav$^{-/-}$ tumors than in Cav$^{+/+}$ tumors (Figure 2, A and B).

Tumors Grown in Cav$^{-/-}$ Mice Present an Elevated IFP and Accumulate High Levels of Fibrinogen in the Early Stages of Development

To understand the apparent resistance to increased permeability in Cav$^{-/-}$ tumors (versus Cav$^{-/-}$ healthy tissues), we next searched for a possible difference in tumor IFP. Using the wick-in-needle technique, we found a net increase in IFP in Cav$^{-/-}$ tumors (versus size-matched Cav$^{+/+}$ tumors) (Figure 3A); this invasive measurement was only possible in large tumors (9-mm diameter). To examine whether an excess extracellular matrix could account for this difference, we evaluated the pres-

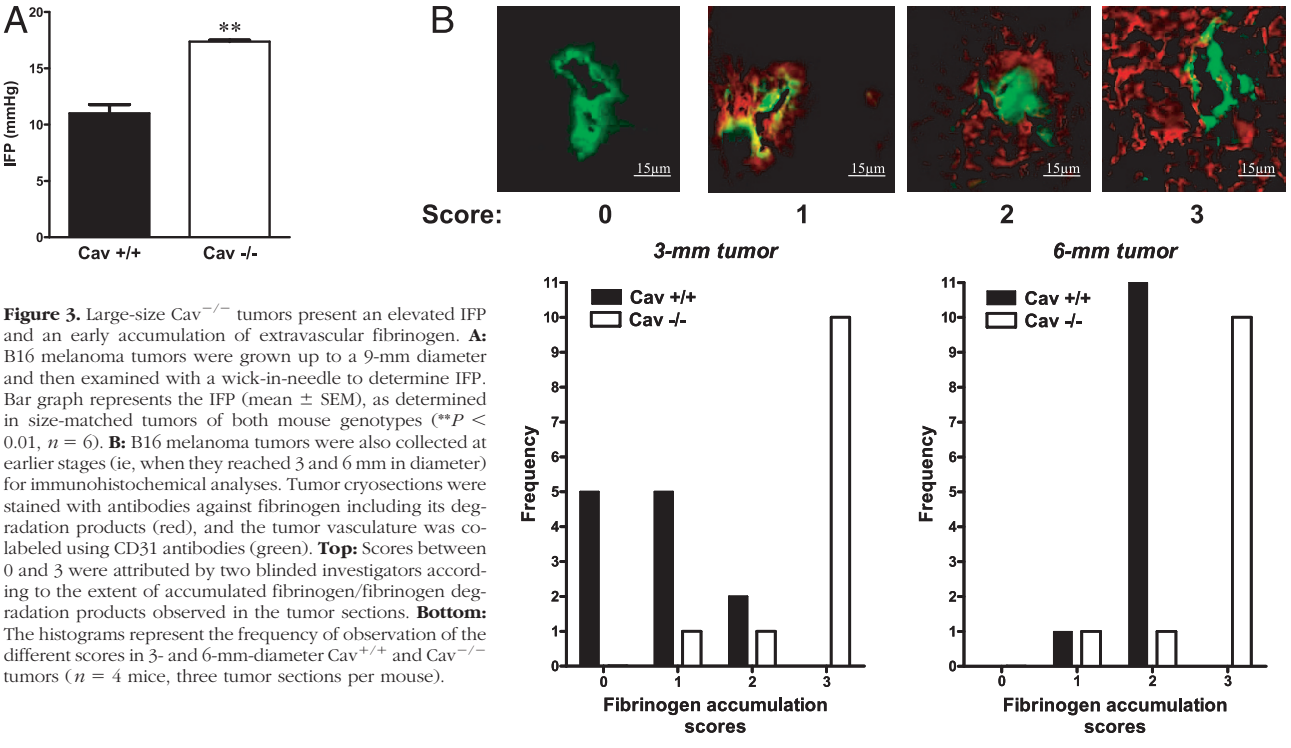

Figure 3. Large-size Cav$^{-/-}$ tumors present an elevated IFP and an early accumulation of extravascular fibrinogen. **A:** B16 melanoma tumors were grown up to a 9-mm diameter and then examined with a wick-in-needle to determine IFP. Bar graph represents the IFP (mean ± SEM), as determined in size-matched tumors of both mouse genotypes (**$P < 0.01$, $n = 6$). **B:** B16 melanoma tumors were also collected at earlier stages (ie, when they reached 3 and 6 mm in diameter) for immunohistochemical analyses. Tumor cryosections were stained with antibodies against fibrinogen including its degradation products (red), and the tumor vasculature was co-labeled using CD31 antibodies (green). **Top:** Scores between 0 and 3 were attributed by two blinded investigators according to the extent of accumulated fibrinogen/fibrinogen degradation products observed in the tumor sections. **Bottom:** The histograms represent the frequency of observation of the different scores in 3- and 6-mm-diameter Cav$^{+/+}$ and Cav$^{-/-}$ tumors ($n = 4$ mice, three tumor sections per mouse).

ence of fibrinogen and its degradation products in sections of tumors collected at different sizes (3-, 6-, and 9-mm diameters). The scoring of the amounts of immunolabeled fibrinogen/fibrinogen degradation products in tumors (see examples on the top of Figure 3B) revealed that fibrinogen accumulation was larger in $Cav^{-/-}$ than in $Cav^{+/+}$ mice (Figure 3B, bottom). It is important to note that these differences were already detectable and eventually more prominent in small tumors (3-mm diameter) (Figure 3B, bottom left), indicating that in the early stages of tumor growth in $Cav^{-/-}$ mice, vessel leakiness was more elevated than in $Cav^{+/+}$ tumors. Higher scores of fibrinogen accumulation were also found in 6-mm $Cav^{-/-}$ tumors (see Figure 3B, bottom right), thereby supporting the elevated IFP observed in large tumors (Figure 3A). Of note, the increasing extent of necrosis rendered difficult the interpretation of the fibrinogen staining in the largest 9-mm-diameter tumors (not shown).

The $Cav^{-/-}$ Tumor Vasculature Presents a High Angiogenic Pattern and a Poor Mural Cell Coverage

We then aimed to identify alterations in the $Cav^{-/-}$ tumor vasculature that could account for the increased tumor V_p and IFP values. The combined use of antibodies directed against α-smooth muscle actin (α-SMA) and CD31 unraveled a dramatic difference both in the general pattern of the tumor vasculature and in the density of mural cells between $Cav^{-/-}$ and $Cav^{+/+}$ mice (Figure 4A). First, the distribution and the size of tumor CD31-positive structures were homogenous in $Cav^{+/+}$ mice but very dependent on the tumor topography in $Cav^{-/-}$ mice. In the latter, large and tortuous vascular structures were observed at the tumor periphery whereas a dense pattern of very small vessels was found in the core of the tumors (see red staining in the single- and dual-color panels in Figure 4A). Regardless of the tumor regions, the CD31-positive staining area in $Cav^{-/-}$ tumors was 2.6-fold larger than in $Cav^{+/+}$ tumors ($P < 0.01$, $n = 5$, 10 sections per mouse). Second, α-SMA-positive staining was associated with a large proportion of CD31-labeled tumor vascular structures in $Cav^{+/+}$ mice but was generally lacking around tumor endothelial structures in $Cav^{-/-}$ mice, independently of the central or peripheral location within the tumor (see green staining in Figure 4A). A scoring procedure led two blinded investigators to estimate that at least 50% of the tumor CD31-positive structures were in close contact with α-SMA-positive mural cells in any tumor-bearing $Cav^{+/+}$ mice (five of five mice; 10 sections analyzed per mouse) whereas only one of five $Cav^{-/-}$ mice presented >50% mural cell coverage.

We also determined whether the higher angiogenic status of tumors established in $Cav^{-/-}$ mice could impact on their growth. Note that in the above experiments, size-matched and not time-matched tumors were compared. Figure 4B shows that a positive difference in the tumor diameter progressively installed between the two mouse genotypes. Accordingly, 18 days after tumor cell injection, tumor growth tended to plateau in $Cav^{+/+}$ mice whereas it continued to progress in $Cav^{-/-}$ mice. In another series of experiments, we also used luciferase-encoding B16 melanoma cells to detect early tumor mass formation by *in vivo* bioluminescence. Figure 4C shows that the tumors grown in $Cav^{-/-}$ mice were more rapidly detectable on luciferin injection (than those grown in $Cav^{+/+}$ mice), confirming the direct positive impact of caveolin deficiency on tumor growth.

Silencing Caveolin-1 Prevents the Migration of SMCs/Pericytes and Naturally Occurs in Vivo *in the Tumor Vasculature*

To explore further the role of caveolin in the recruitment of mural cells, we used cultures of SMC/pericyte precursors (10T1/2 cells) and evaluated their migration capacity in an *in vitro* wound assay. We first examined the changes in caveolin subcellular localization during 10T1/2 cell migration, a previously described hallmark of the caveolin implication in endothelial cell migration. Figure 5A shows that from a diffuse location in quiescent, confluent cells, caveolin-1 presented a polarized distribution during migration. Caveolin-1 could be found in the cell nuclei and at the rear of migrating 10T1/2 cells, just at the opposite of the migratory front. We then used small interfering RNA to silence caveolin-1 expression in 10T1/2 cells and examined the migratory capacity of these cells in the wound assay. As shown in Figure 5B, a 75% inhibition of caveolin expression led to a significant reduction in the migration of 10T1/2 cells; this effect was confirmed using a second siRNA and persisted for at least 72 hours (not shown).

To determine whether the down-regulation of caveolin was a biological phenomenon naturally occurring in the tumor microenvironment, we compared the expression of caveolin in microvessels of $Cav^{+/+}$ mice after injection (or not) of B16 melanoma cells in their direct vicinity. These vessels (ie, saphenous arterioles and downstream branches) were dissected after 2 weeks of tumor growth and isolated from the tumor stroma (wherein they were completely trapped). Figure 5C shows that a significant reduction in caveolin expression could be authenticated in the microvessels influenced by the tumor microenvironment versus size-matched control microvessels isolated from the contralateral leg.

The Lack of Caveolin Inhibits the Basal and Platelet-Derived Growth Factor (PDGF)-Driven Mobilization of SMCs/Myofibroblasts

To explore further a possible lack of mural cell migration/recruitment during the angiogenic process in $Cav^{-/-}$ mice, we also used an *ex vivo* assay based on the three-dimensional culture of aorta rings in collagen gels. This assay allows simultaneous evaluation of the organization of proliferating EC in tubes (see rectilinear structures in Figure 6, A and C) and the outgrowth of myofibroblasts/SMCs (see scattered cells in Figure 6, A and C). Figure 6A shows that a significantly higher number of endothelial

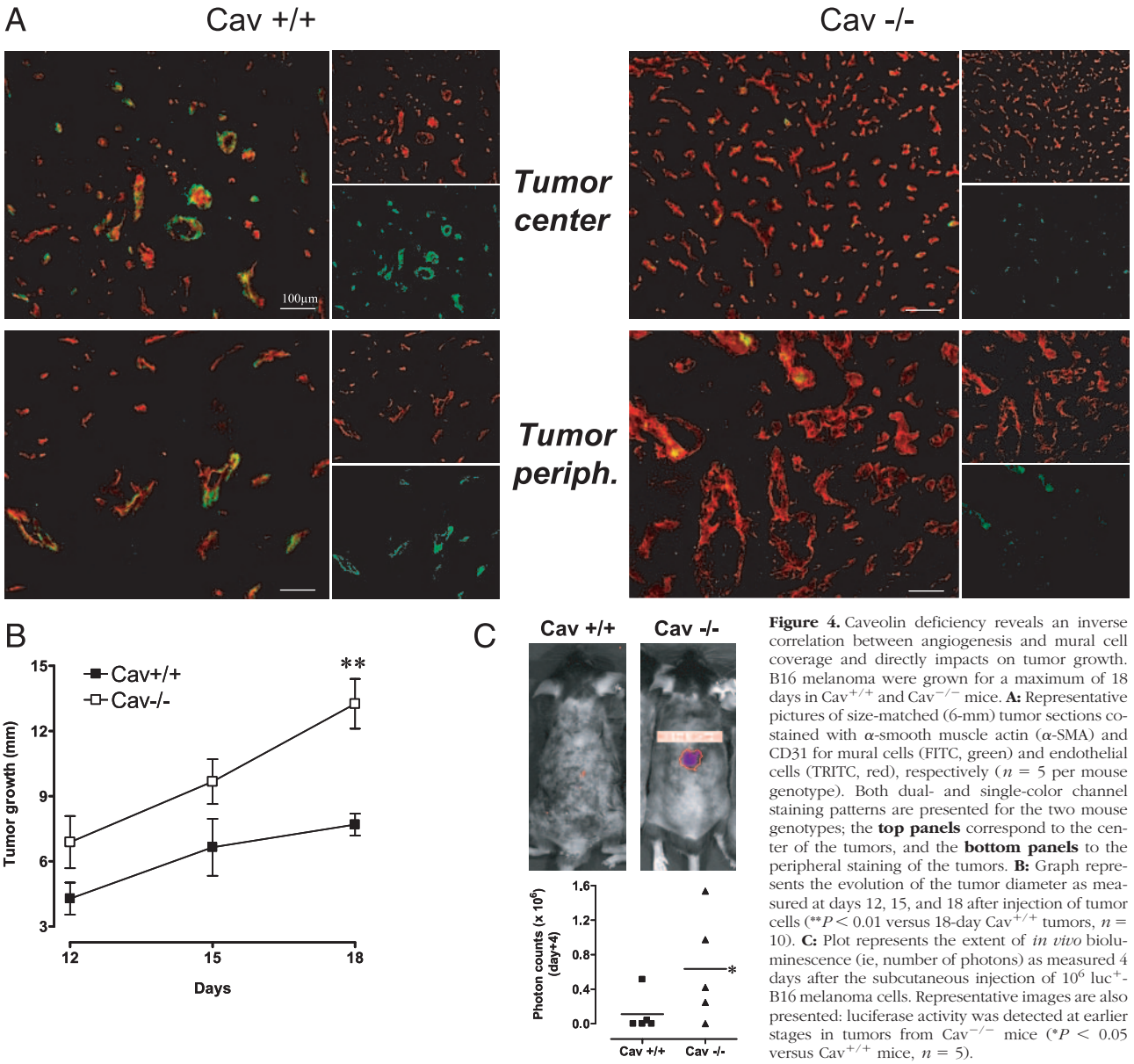

Figure 4. Caveolin deficiency reveals an inverse correlation between angiogenesis and mural cell coverage and directly impacts on tumor growth. B16 melanoma were grown for a maximum of 18 days in $Cav^{+/+}$ and $Cav^{-/-}$ mice. **A:** Representative pictures of size-matched (6-mm) tumor sections co-stained with α-smooth muscle actin (α-SMA) and CD31 for mural cells (FITC, green) and endothelial cells (TRITC, red), respectively ($n = 5$ per mouse genotype). Both dual- and single-color channel staining patterns are presented for the two mouse genotypes; the **top panels** correspond to the center of the tumors, and the **bottom panels** to the peripheral staining of the tumors. **B:** Graph represents the evolution of the tumor diameter as measured at days 12, 15, and 18 after injection of tumor cells ($^{**}P < 0.01$ versus 18-day $Cav^{+/+}$ tumors, $n = 10$). **C:** Plot represents the extent of *in vivo* bioluminescence (ie, number of photons) as measured 4 days after the subcutaneous injection of 10^6 luc^+-B16 melanoma cells. Representative images are also presented: luciferase activity was detected at earlier stages in tumors from $Cav^{-/-}$ mice ($^{*}P < 0.05$ versus $Cav^{+/+}$ mice, $n = 5$).

tubes formed from $Cav^{-/-}$ aorta rings, reflecting a higher intrinsic angiogenic potential (Figure 6B, left). Conversely, the amounts of scattered myofibroblasts/SMCs were approximately twofold less around the $Cav^{-/-}$ aorta rings than the $Cav^{+/+}$ aorta (Figure 6B, right).

We then aimed to determine whether a major signaling cascade involved in mural cell recruitment, namely the PDGF axis, was altered in $Cav^{-/-}$ mice. The data presented in Figure 6C show that although PDGF stimulated a dramatic outgrowth of SMCs/myofibroblasts from the $Cav^{+/+}$ aorta ring, a limited amount of these scattered cells could be identified around the $Cav^{-/-}$ aorta rings (see also bar graph in Figure 6C). Note also that the endothelial tubes nicely formed from the PDGF-exposed $Cav^{-/-}$ aorta rings but not from the $Cav^{+/+}$ aorta explants (Figure 6C, top). Finally, to validate the alterations in PDGF signaling, we examined the phosphorylation status of Akt, a well-known kinase located downstream PDGF stimulation. Figure 6D shows that the extent of Akt activation (ie, phosphorylation) was dramatically reduced in SMCs outgrown from $Cav^{-/-}$ aorta rings.

Discussion

This study provides a new mechanistic rationale to support a link between caveolin down-modulation and the development of the tumor neovasculature. A first clue in the biological role of caveolin down-regulation is the increase in tumor vessel leakiness that we could substantiate in the early steps of tumor progression in $Cav^{-/-}$ mice by the accumulation of fibrinogen and its degradation products (versus size-matched tumors in wild-type mice) (Figure 3B). The absence of caveolae in lung capillaries of caveolin-deficient mice was previously reported to be associated with an increase in vascular permeabil-

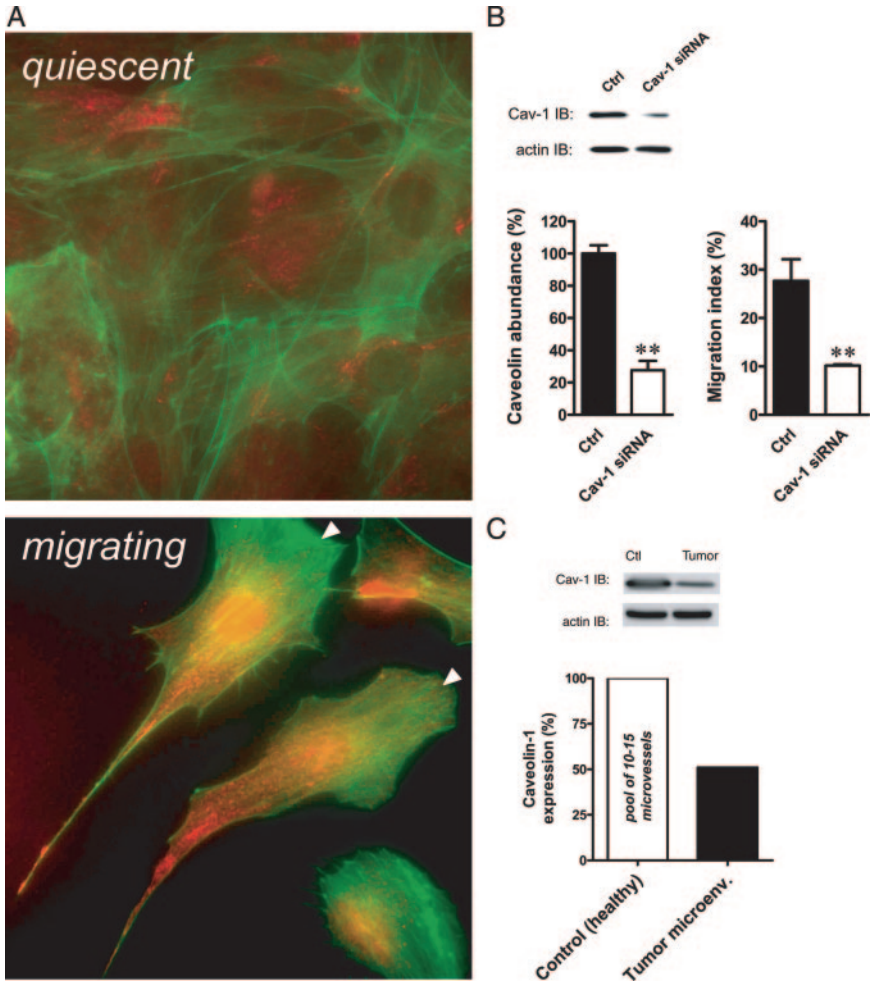

Figure 5. Silencing caveolin-1 reduces the extent of SMC/pericyte migration and naturally occurs *in vivo*. **A:** 10T1/2 cells were grown to confluence and after serum deprivation for 24 hours, a wound assay was performed by scrapping out a 0.5-mm-wide band of cells. Representative picture of migrating (ie, present in the wounded area 24 hours later) and nonmigrating (within the confluent monolayer far from the wound) SMC/pericyte precursor cells as observed by immunofluorescence using caveolin-1 antibodies (TRITC detection, red) and FITC-phalloidin (green). Note that the caveolin subcellular distribution is polarized at the rear of migrating cells (ie, at the opposite of the migration front, **arrowheads**). **B:** Bar graph represent the effects of a siRNA targeting caveolin (sequence 206 to 226: AAGATGTGATTGCAGAACCAG) on the protein expression of caveolin (**left**) and on the migration of SMC/pericyte precursors (**right**); data are the means ± SEM of the caveolin expression and of the migration index (see Materials and Methods) determined in three independent experiments, respectively (**$P < 0.01$). A representative caveolin immunoblot (IB) is also shown to validate the silencing of caveolin expression (versus control, scramble RNA) in our experimental conditions. **C:** Representative immunoblots and bar graph show the levels of caveolin expression in pools of 10 to 15 microvessels microdissected from B16 melanoma established (2 weeks before) by injection of tumor cells at the vicinity of the saphenous arteriole in $Cav^{+/+}$ mice; size-matched microvessels isolated from the contralateral (tumor-free) leg were used as control to validate the down-regulation of caveolin-1 in tumor microvessels. This experiment was repeated twice with similar results.

ity.[32] Our study now documents that the phenomenon is exacerbated and accelerated in tumors (see detection of excess fibrinogen as early as in 3-mm tumors) but is then progressively buffered by the consecutive increase in IFP (Figure 3A). Indeed, at the time an elevated vascular permeability is still detectable in healthy tissues (Figure 1A), extravasation of radioiodinated albumin in tumors did not differ between $Cav^{-/-}$ and $Cav^{+/+}$ mice (Figure 1A), neither were the permeability constants K_{trans} and K_{ep} different between the two mouse genotypes, as determined by DCE-MRI (Figure 2). Moreover, we found that in $Cav^{+/+}$ mice, the tumor growth was associated with a decrease in the abundance of caveolin in tumor-perfusing microvessels (Figure 5C), confirming previous observations of a down-regulation of caveolin in angiogenic endothelial cells.[16–20] Altogether, these data support a pathogenic link between the caveolin down-regulation that occurs naturally in the tumor microvasculature and the dynamic increase in vessel permeability to plasma proteins known to lead to the production of a scaffold provisional matrix for cell migration.

A second key step in the development of tumor vascularization that seemed to be regulated by the caveolin down-regulation is the dynamic process of tumor vessel maturation. During embryogenesis and in the rare circumstances of the adult life in which angiogenesis is switched on, neoformed endothelial tubes are rapidly covered by mural cells to give rise to mature blood vessels gifted with vasomotion.[5] In tumors, the imbalance between the levels of pro- and anti-angiogenic molecules tends to promote a continuous remodeling of the tumor vasculature.[4,5,33,34] In the current study, the lack of caveolin was shown to prevent the recruitment of α-SMA-positive mural cells in growing tumors, a phenomenon

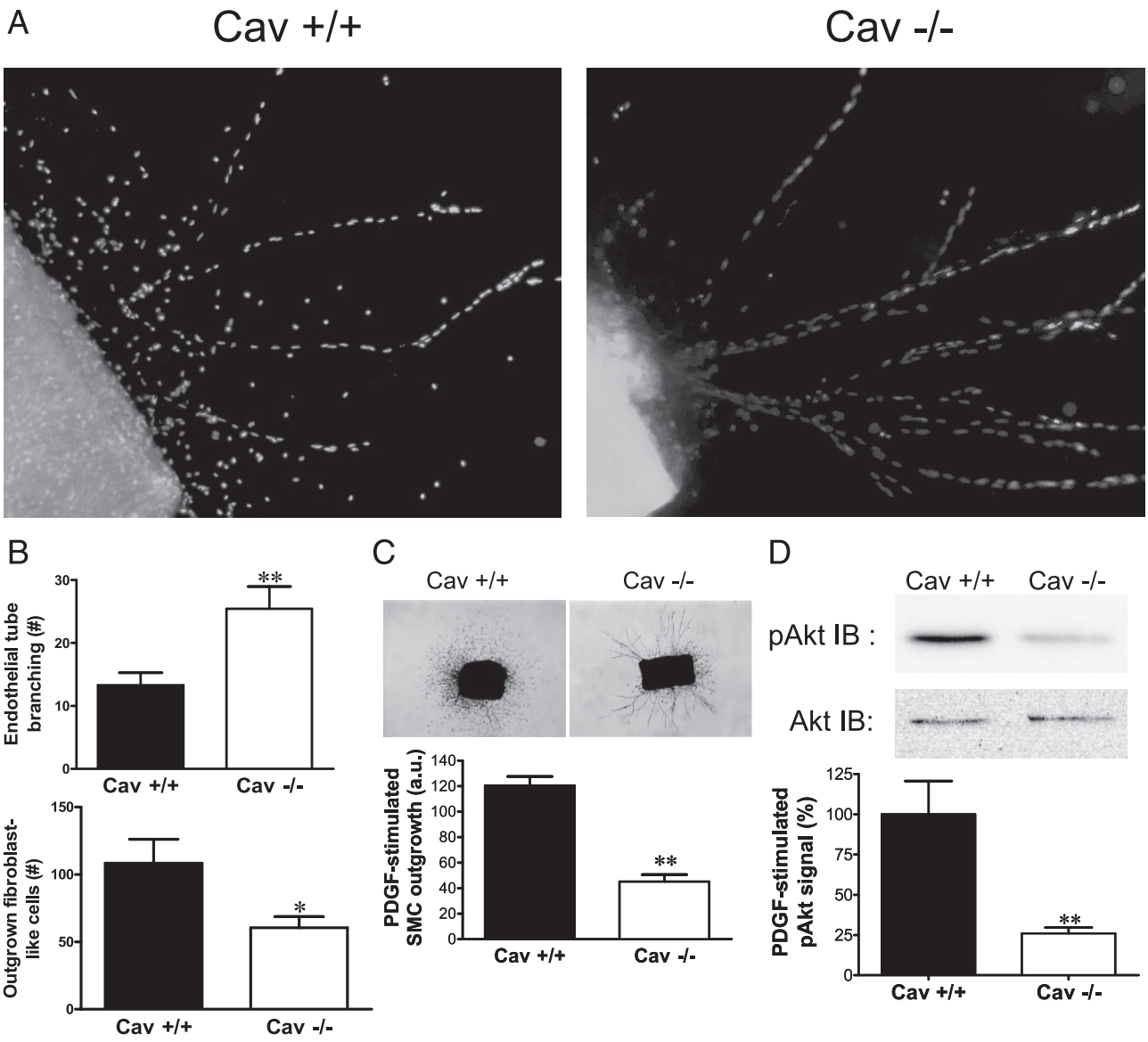

Figure 6. Caveolin deficiency promotes endothelial tube formation and prevents both basal and PDGF-stimulated SMC/myofibroblast outgrowth. **A:** Photomicrographs show the angiogenic response of 12-day cultured collagen-embedded thoracic aorta ring explants from $Cav^{+/+}$ and $Cav^{-/-}$ mice. The linear organization of endothelial tubes allows discrimination of the corresponding DAPI-stained endothelial cell nuclei from the more dispersed ones belonging to SMCs/myofibroblasts (ie, cells not stained with endothelial cell markers such as CD31 or MECA32 antibodies, not shown). **B:** Bar graphs represent the numbers of endothelial branching sprouts per aortic rings (**top**) and the number of SMCs/myofibroblasts (**bottom**); $^{*}P < 0.05$, $^{**}P < 0.01$, $n = 10$ aorta rings per mouse genotype. **C: Top:** Photomicrographs show the effects of PDGF-BB (30 ng/ml) on the outgrowth of SMCs/myofibroblasts from $Cav^{+/+}$ and $Cav^{-/-}$ aorta ring explants; note the inverse relationship between the proliferation of these cells and the extent of endothelial tube formation. **Bottom:** Bar graph represents the extent of SMC/myofibroblast outgrowth determined by measuring the mean distance between these cells and the explant ($^{**}P < 0.01$, $n = 5$ aorta rings per mouse genotype). **D:** Representative immunoblot analysis (**top**) and quantification (**bottom**) of phospho-Akt and Akt in SMCs/myofibroblasts (isolated from $Cav^{+/+}$ and $Cav^{-/-}$ aorta rings) after a 20-minute exposure to PDGF-BB (30 ng/ml) ($^{**}P < 0.01$, $n = 3$ per mouse genotype).

that we found associated with a higher density of endothelial structures in the center of $Cav^{-/-}$ tumors (Figure 4A). The lack of vessel maturation in $Cav^{-/-}$ tumors also translated at the tumor periphery in the development of very large, tortuous vessels, supporting the concept of a continuous endothelial growth in absence of a minimal recruitment of mural cells. DCE-MRI confirmed that the blood plasma volume (V_p) was significantly increased in $Cav^{-/-}$ tumors in good correlation with the higher density and/or size of neovessels in these mice (Figure 4). Of note, a small but significant increase in B16 melanoma growth rate was observed in $Cav^{-/-}$ mice (versus $Cav^{+/+}$ mice) (Figure 4, B and C), likely to reflect the higher angiogenic status of $Cav^{-/-}$ tumors.

To establish further the link between caveolin down-regulation and tumor vessel immaturity, we also used *in vitro* migration and vascular morphogenesis assays. We showed that SMC/pericyte precursor 10T1/2 cells treated with a silencing caveolin siRNA presented a defect in their capacity to migrate and that more endothelial tubes and lesser outgrowth of myofibroblasts arose from $Cav^{-/-}$ aorta rings. These assays also led us to identify clues in the defective $Cav^{-/-}$ vessel morphogenesis. We found that in nontransduced SMC/

pericyte precursors, caveolin was polarized at the rear of the cell during migration, strongly suggesting a dynamic role in cell migration, such as the prevention of lamellipod protrusion as previously reported in endothelial cells.[35] Among the possible effectors that master vessel maturation,[36] we also showed that the PDGF signaling pathway was altered in $Cav^{-/-}$ SMCs. PDGF is the prototypical growth factor released by proliferating endothelial cells to recruit mural cells to stop ongoing angiogenesis.[37] In our study, we found that the capacity of PDGF-B to stimulate SMCs and myofibroblasts outgrowth in the aorta ring assay (Figure 6C) as well as the stimulation of the downstream kinase Akt (Figure 6D) were lost in the absence of caveolin. Altogether and although alterations in other pathways than PDGF are likely to be involved in the observed $Cav^{-/-}$ vascular phenotype, our data indicate that caveolin is a master regulator of the maturation of tumor blood vessels.

Hassan and colleagues[38] recently reported that caveolin-deficient SMCs presented cell autonomous abnormalities in proliferation and migration. In addition, in another study by the same authors, caveolin down-regulation was shown to favor activation of signal transduction pathways usually associated with SMC proliferation such as extracellular signal-regulated kinase phosphorylation.[39] Although obvious differences in the biological context of the down-regulation of caveolin in these studies may account for the discrepancies with our study, another explanation may also be found in the double role of caveolin, ie, blocking the basal activity of enzymes residing in caveolae but facilitating their activation on agonist stimulation.[40,41] In other words, the deficiency in caveolin/caveolae may lead either to a tonic activation of these signaling enzymes in the absence of stimuli (or in response to stimulatory pathways not concentrated in caveolae), or inversely to an incapacity to transmit the signal because of the deficit in the caveolar compartmentation of the different actors. This so-called caveolae paradox may explain why $Cav^{-/-}$ SMC proliferation was found to be associated with an increased extracellular signal-regulated kinase activation in basal conditions[39] or in response to the noncaveolar ETB receptor stimulation,[38] whereas in other studies[42] (including ours) stimulation of the caveolar PDGFR-β receptor led to a lesser activation of extracellular signal-regulated kinase or Akt in SMCs exposed to caveolin siRNA.

Finally, Woodman and colleagues[43] have reported a defect in tumor angiogenesis in caveolin-deficient mice using the same syngeneic B16 melanoma model. In this study, however, they evaluated angiogenesis by vessel counting from hematoxylin and eosin-stained paraffin-embedded sections. The mural cell-free endothelial structures and immature vascular morphology may have led these authors to underestimate the extent of tumor angiogenesis in caveolin-deficient mice. In our hands, the stimulated angiogenic process was only detectable through the use of specific immunomarkers, including von Willebrand factor, MECA32, and CD31 antibodies, to probe endothelial structures within the tumor mass (as reported in Figure 4A).

In conclusion, our study emphasizes the close relationship between mural cell recruitment and termination of angiogenesis. One generally admitted view is that tumor vessel maturation is incomplete because the exponential growth of endothelial structures beats the capacity of pericytes/SMCs to be recruited in time and in numbers to sufficiently cover neoformed endothelial tubes.[33] Here, our study supports another (although nonexclusive) reading of this phenomenon in which the defect in vessel maturation would, in fact, be actively supported by the dynamic down-regulation of caveolin. Furthermore, our data underscore how caveolin deficiency contributes through an early increase in tumor vessel permeability to build up an extravascular matrix network that promotes angiogenesis. Thus, the previously reported angiogenic growth factor-driven decrease in caveolin abundance[16,17] supports the advantages of an increased endothelium permeability, the stimulation of EC proliferation/migration and the prevention of the angiogenic process termination by mural cell recruitment. Caveolin-1 has therefore the potential to be an important prognostic indicator in delineating the degree of tumor vessel maturity and thereby the therapeutic efficacy of anti-angiogenic drugs.

Acknowledgments

We thank F. Kostet, H. Esfahani, and D. De Mulder for excellent technical assistance.

References

1. Hashizume H, Baluk P, Morikawa S, McLean JW, Thurston G, Roberge S, Jain RK, McDonald DM: Openings between defective endothelial cells explain tumor vessel leakiness. Am J Pathol 2000, 156:1363–1380
2. Less JR, Skalak TC, Sevick EM, Jain RK: Microvascular architecture in a mammary carcinoma: branching patterns and vessel dimensions. Cancer Res 1991, 51:265–273
3. Hobbs SK, Monsky WL, Yuan F, Roberts WG, Griffith L, Torchilin VP, Jain RK: Regulation of transport pathways in tumor vessels: role of tumor type and microenvironment. Proc Natl Acad Sci USA 1998, 95:4607–4612
4. McDonald DM, Baluk P: Significance of blood vessel leakiness in cancer. Cancer Res 2002, 62:5381–5385
5. Jain RK: Molecular regulation of vessel maturation. Nat Med 2003, 9:685–693
6. Heldin CH, Rubin K, Pietras K, Ostman A: High interstitial fluid pressure—an obstacle in cancer therapy. Nat Rev Cancer 2004, 4:806–813
7. Jain RK: Normalization of tumor vasculature: an emerging concept in antiangiogenic therapy. Science 2005, 307:58–62
8. Lammerts E, Roswall P, Sundberg C, Gotwals PJ, Koteliansky VE, Reed RK, Heldin NE, Rubin K: Interference with TGF-β1 and -β3 in tumor stroma lowers tumor interstitial fluid pressure independently of growth in experimental carcinoma. Int J Cancer 2002, 102:453–462
9. Stoeltzing O, Ahmad SA, Liu W, McCarty MF, Wey JS, Parikh AA, Fan F, Reinmuth N, Kawaguchi M, Bucana CD, Ellis LM: Angiopoietin-1 inhibits vascular permeability, angiogenesis, and growth of hepatic colon cancer tumors. Cancer Res 2003, 63:3370–3377
10. Frank PG, Woodman SE, Park DS, Lisanti MP: Caveolin, caveolae, and endothelial cell function. Arterioscler Thromb Vasc Biol 2003, 23:1161–1168

11. Schubert W, Frank PG, Razani B, Park DS, Chow CW, Lisanti MP: Caveolae-deficient endothelial cells show defects in the uptake and transport of albumin in vivo. J Biol Chem 2001, 276:48619–48622
12. Brouet A, DeWever J, Martinive P, Havaux X, Bouzin C, Sonveaux P, Feron O: Antitumor effects of in vivo caveolin gene delivery are associated with the inhibition of the proangiogenic and vasodilatory effects of nitric oxide. FASEB J 2005, 19:602–604
13. Gratton JP, Lin MI, Yu J, Weiss ED, Jiang ZL, Fairchild TA, Iwakiri Y, Groszmann R, Claffey KP, Cheng YC, Sessa WC: Selective inhibition of tumor microvascular permeability by cavtratin blocks tumor progression in mice. Cancer Cell 2003, 4:31–39
14. Labrecque L, Royal I, Surprenant DS, Patterson C, Gingras D, Beliveau R: Regulation of vascular endothelial growth factor receptor-2 activity by caveolin-1 and plasma membrane cholesterol. Mol Biol Cell 2003, 14:334–347
15. Sonveaux P, Martinive P, DeWever J, Batova Z, Daneau G, Pelat M, Ghisdal P, Gregoire V, Dessy C, Balligand JL, Feron O: Caveolin-1 expression is critical for vascular endothelial growth factor-induced ischemic hindlimb collateralization and nitric oxide-mediated angiogenesis. Circ Res 2004, 95:154–161
16. Régina A, Jodoin J, Khoueir P, Rolland Y, Berthelet F, Moumdjian R, Fenart L, Cecchelli R, Demeule M, Beliveau R: Down-regulation of caveolin-1 in glioma vasculature: modulation by radiotherapy. J Neurosci Res 2004, 75:291–299
17. Liu J, Razani B, Tang S, Terman BI, Ware JA, Lisanti MP: Angiogenesis activators and inhibitors differentially regulate caveolin-1 expression and caveolae formation in vascular endothelial cells. Angiogenesis inhibitors block vascular endothelial growth factor-induced down-regulation of caveolin-1. J Biol Chem 1999, 274:15781–15785
18. Liu J, Wang XB, Park DS, Lisanti MP: Caveolin-1 expression enhances endothelial capillary tubule formation. J Biol Chem 2002, 277:10661–10668
19. Phillips PG, Birnby LM: Nitric oxide modulates caveolin-1 and matrix metalloproteinase-9 expression and distribution at the endothelial cell/tumor cell interface. Am J Physiol 2004, 286:L1055–L1065
20. Sonveaux P, Brouet A, Havaux X, Gregoire V, Dessy C, Balligand JL, Feron O: Irradiation-induced angiogenesis through the up-regulation of the nitric oxide pathway: implications for tumor radiotherapy. Cancer Res 2003, 63:1012–1019
21. Ray JL, Leach R, Herbert JM, Benson M: Isolation of vascular smooth muscle cells from a single murine aorta. Methods Cell Sci 2001, 23:185–188
22. Boucher Y, Kirkwood JM, Opacic D, Desantis M, Jain RK: Interstitial hypertension in superficial metastatic melanomas in humans. Cancer Res 1991, 51:6691–6694
23. Baudelet C, Cron GO, Gallez B: Determination of the maturity and functionality of tumor vasculature by MRI: correlation between BOLD-MRI and DCE-MRI using P792 in experimental fibrosarcoma tumors. Magn Reson Med 2006, 56:1041–1049
24. Martinive P, De Wever J, Bouzin C, Baudelet C, Sonveaux P, Gregoire V, Gallez B, Feron O: Reversal of temporal and spatial heterogeneities in tumor perfusion identifies the tumor vascular tone as a tunable variable to improve drug delivery. Mol Cancer Ther 2006, 5:1620–1627
25. Crokart N, Jordan BF, Baudelet C, Cron GO, Hotton J, Radermacher K, Gregoire V, Beghein N, Martinive P, Bouzin C, Feron O, Gallez B: Glucocorticoids modulate tumor radiation response through a decrease in tumor oxygen consumption. Clin Cancer Res 2007, 13:630–635
26. Ansiaux R, Baudelet C, Jordan BF, Beghein N, Sonveaux P, De Wever J, Martinive P, Gregoire V, Feron O, Gallez B: Thalidomide radiosensitizes tumors through early changes in the tumor microenvironment. Clin Cancer Res 2005, 11:743–750
27. Su MY, Jao JC, Nalcioglu O: Measurement of vascular volume fraction and blood-tissue permeability constants with a pharmacokinetic model: studies in rat muscle tumors with dynamic Gd-DTPA enhanced MRI. Magn Reson Med 1994, 32:714–724
28. Tofts PS: Modeling tracer kinetics in dynamic Gd-DTPA MR imaging. J Magn Reson Imaging 1997, 7:91–101
29. Sonveaux P, Frerart F, Bouzin C, Brouet A, DeWever J, Jordan BF, Gallez B, Feron O: Irradiation promotes Akt-targeting therapeutic gene delivery to the tumor vasculature. Int J Radiat Oncol Biol Phys 2007, 67:1155–1162
30. Sonveaux P, Dessy C, Martinive P, Havaux X, Jordan BF, Gallez B, Gregoire V, Balligand JL, Feron O: Endothelin-1 is a critical mediator of myogenic tone in tumor arterioles: implications for cancer treatment. Cancer Res 2004, 64:3209–3214
31. Blacher S, Devy L, Burbridge MF, Roland G, Tucker G, Noel A, Foidart JM: Improved quantification of angiogenesis in the rat aortic ring assay. Angiogenesis 2001, 4:133–142
32. Schubert W, Frank PG, Woodman SE, Hyogo H, Cohen DE, Chow CW, Lisanti MP: Microvascular hyperpermeability in caveolin-1 (−/−) knock-out mice. Treatment with a specific nitric-oxide synthase inhibitor, L-name, restores normal microvascular permeability in Cav-1 null mice. J Biol Chem 2002, 277:40091–40098
33. Morikawa S, Baluk P, Kaidoh T, Haskell A, Jain RK, McDonald DM: Abnormalities in pericytes on blood vessels and endothelial sprouts in tumors. Am J Pathol 2002, 160:985–1000
34. Baluk P, Morikawa S, Haskell A, Mancuso M, McDonald DM: Abnormalities of basement membrane on blood vessels and endothelial sprouts in tumors. Am J Pathol 2003, 163:1801–1815
35. Parat MO, Anand-Apte B, Fox PL: Differential caveolin-1 polarization in endothelial cells during migration in two and three dimensions. Mol Biol Cell 2003, 14:3156–3168
36. Chantrain CF, Henriet P, Jodele S, Emonard H, Feron O, Courtoy PJ, DeClerck YA, Marbaix E: Mechanisms of pericyte recruitment in tumour angiogenesis: a new role for metalloproteinases. Eur J Cancer 2006, 42:310–318
37. Lindahl P, Johansson BR, Leveen P, Betsholtz C: Pericyte loss and microaneurysm formation in PDGF-B-deficient mice. Science 1997, 277:242–245
38. Hassan GS, Williams TM, Frank PG, Lisanti MP: Caveolin-1-deficient aortic smooth muscle cells show cell autonomous abnormalities in proliferation, migration, and endothelin-based signal transduction. Am J Physiol 2006, 290:H2393–H2401
39. Hassan GS, Jasmin JF, Schubert W, Frank PG, Lisanti MP: Caveolin-1 deficiency stimulates neointima formation during vascular injury. Biochemistry 2004, 43:8312–8321
40. Feron O, Kelly RA: The caveolar paradox: suppressing, inducing, and terminating eNOS signaling. Circ Res 2001, 88:129–131
41. Sbaa E, Frerart F, Feron O: The double regulation of endothelial nitric oxide synthase by caveolae and caveolin: a paradox solved through the study of angiogenesis. Trends Cardiovasc Med 2005, 15:157–162
42. Gosens R, Stelmack GL, Dueck G, McNeill KD, Yamasaki A, Gerthoffer WT, Unruh H, Gounni AS, Zaagsma J, Halayko AJ: Role of caveolin-1 in p42/p44 MAP kinase activation and proliferation of human airway smooth muscle. Am J Physiol 2006, 291:L523–L534
43. Woodman SE, Ashton AW, Schubert W, Lee H, Williams TM, Medina FA, Wyckoff JB, Combs TP, Lisanti MP: Caveolin-1 knockout mice show an impaired angiogenic response to exogenous stimuli. Am J Pathol 2003, 162:2059–2068